ABSTRACT

Title of Thesis: NONLINEAR KINETICS MODEL OF CONCRETE DAMAGE DUE TO DELAYED ETTRINGITE FORMATION

Nour Alkhalouf,
Master of Science, 2021

Directed By: Professor Amde M. Amde,
Department of Civil and Environmental Engineering

Delayed ettringite formation (DEF) in concrete is a deleterious process characterized by the expansion and cracking of concrete. Recent research has shown that concrete expansion occurs in three consecutive stages and can be fit into a nonlinear model (Feuze, Livingston, & Amde, 2019). This paper used data from tests conducted previously by the University of Maryland on concrete prisms with varying potassium contents, types of fine aggregates, and exposure conditions. Test results were fit into a nonlinear model developed by Feuze et al. (2019). The model, referred to in this research as “The Nonlinear Kinetics Model”, is a four-parameter model that conveys the time dependence of the expansion of concrete due to DEF. Results have shown the nonlinear kinetics model previously developed and tested by Feuze et al. (2019) in one set of conditions, can be applied to more DEF experiments with a variety of other

conditions. Thus, the model parameters can provide a framework for comparing the effects of various factors that influence DEF.

NONLINEAR KINETICS MODEL OF CONCRETE DAMAGE DUE TO DELAYED ETTRINGITE FORMATION

By

Nour Alkhalouf

Thesis submitted to the Faculty of the Graduate School of the
University of Maryland, College Park in partial fulfillment
of the requirements for the degree of
Master of Science
2021

Advisory Committee:

Professor Amde M. Amde, Chair/Advisor
Professor Mohamed S. Aggour
Professor Chung C. Fu

Acknowledgements

I would first like to thank my advisor, Dr. Amde M. Amde, for his support, guidance, and suggestions throughout this research.

My sincere gratitude to Dr. Richard Livingston, Adjunct Professor, at Materials Science and Engineering Department, at the University of Maryland, College Park, for his continuous support and guidance.

Thanks are also due to Mr. Stuart Sherman and the staff of the National Ready Mix Concrete Association Laboratory for their assistance in preparing and measuring the concrete prisms over the last two and half decades.

I would also like to thank Dr. Jorgmai Ceesay, Dr. Nicolas McMorris, Dr. Amal Azzam, and Kenneth Williams for their research data, which served as the basis for this research.

My deep gratitude also goes to my understanding family for their encouragement and support.

Finally, I dedicate this research to the man who put me on this path, my father. A thank you is an understatement; I hope I made you proud.

Table of Contents

List of Figures

List of Tables

List of Abbreviations and Symbols

DEF……...Delayed Ettringite Formation
ASR……...Alkali-Silica Reaction
ASTM……...American Society for Testing and Materials
EEF……...Early Ettringite Formation
AAR……...Alkali Aggregate Reaction
SEM……...Scanning Electron Microscope
EDAX……...Energy Dispersive Analysis X-ray
K_2CO_3……...Potassium Carbonate
K_2SO_4……...Potassium Sulfate

Chapter 1: Introduction

1.1 Problem Statement

One of the most prominent challenges facing concrete structures today is the premature deterioration process that causes loss of strength and durability in structures. Replacing, rehabilitating, and maintaining these structures has proven to be a challenging and uneconomical task for many cities in North America. For this reason, extensive research has been conducted on the reasons behind premature deterioration in concrete. In these studies, chemical reactions in concrete, which include Alkali-Silica Reactions (ASR) and Delayed Ettringite Formation (DEF), have been identified as one of the main reasons. ASR and DEF cause expansion, which creates voids in concrete resulting in microcracks. **Figure 1.1** shows a precast, prestressed railway tie showing signs of cracking due to DEF. Although ASR and DEF are often found together, DEF can be differentiated from ASR through shape and chemistry. While there is a standardized test through ASTM C1293 that evaluates the potential deterioration in a concrete sample due to ASR, there is no standardized test currently available to test the potential presence of DEF in a concrete sample.

Figure 1.1: Precast, Prestressed Railway Tie Showing Signs of DEF-Induced Cracking

The University of Maryland's database contains substantial data from tests that have been conducted on concrete samples with different cement chemistry, curing methods, and exposure conditions. These tests were performed as part of research investigating the characteristics of DEF and its influence on concrete. To initiate microcracks, the concrete samples were subjected to either heat cycles or freeze-thaw cycles. While many conclusions have been made about DEF through these tests, the time dependence of the expansion of concrete specimens due to DEF can only be fully understood by developing a kinetics model of the data.

1.2 Background

The phenomenon of DEF has been investigated in a significant amount of prior research. Ettringite is often described as a crystalline calcium sulfoaluminate hydrate product of Portland cement (PC) hydration. It consists of the general formula of $3(CaO)\cdot Al_2O_3\cdot 3CaSO_4\cdot 32H_2O$. As shown in **Figure 1.2**, viewing ettringite using scanning electron microscopy demonstrates its needle-like crystal structure (Bollmann & Stark, 1997).

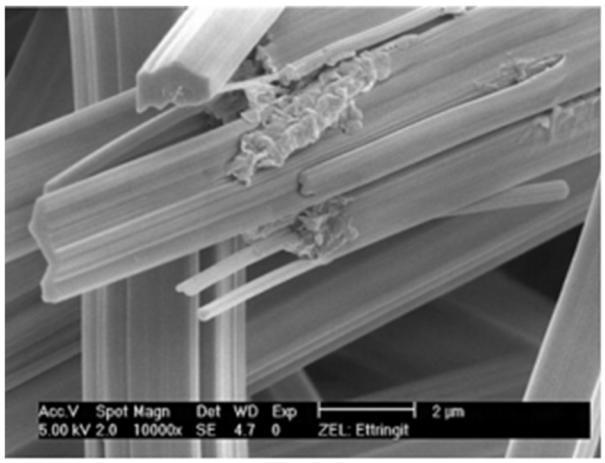

Figure 1.2: Needle-Like Crystal Structure of Ettringite

Ettringite is a product of Portland cement hydration which results from water molecules reacting with the molecules that make up cement (C3S, C2S, C4A, C4AF). These reactions occur when gypsum and additives are added, a process often referred to as early ettringite formation (EEF). Although EEF causes volumetric expansion, it is not considered deleterious, as the cement is still in its plastic state and can accommodate

expansion. On the contrary, Yan, Zheng, Peng, & Qin (2004) have noted that EEF is beneficial to cement since it compensates for the formation that occurs due to concrete shrinkage.

Many factors are regarded as causes of DEF. These factors range from the chemistry of cement, to curing methods, and exposure conditions after curing. The occurrence of DEF can be further explained through two commonly used models: the thermal decomposition model and the holistic approach model (Williams, 2003).

1.2.1 Thermal Decomposition Model

Many researchers have associated the presence of DEF with the curing of precast concrete which takes place at elevated temperatures, usually greater than 70°C, to achieve early concrete strength. Curing concrete at high temperatures has been described as a “heat-induced internal sulphate attack” that results in a high concentration of sulfate in the pores of cement, which is further exacerbated through the heat of hydration of the C_3A and C_3S present (Hooton, Boyd,& Bhadkamkar, 2005). The result of this process is expansion which causes cement paste to move away from coarse aggregate, forming voids in the mix. As expansion advances, these gaps become filled with ettringite.

1.2.2 Holistic Approach Model

While the thermal decomposition model provides a substantial explanation of the process behind DEF, it is limited in that it focuses solely on concrete members that have been exposed to high temperatures.

Collepardi (1999) provides an extensive model that explains the factors behind DEF in all concrete members. The model introduces three main factors that can result in DEF due to an internal sulphate attack: microcracking, late sulfate release, and exposure to water.

- Microcracking: Freeze-thaw cycles, plastic shrinkage, and dynamic service loads are some of the reasons behind the occurrence of microcracks. The holistic model approach assigns microcracks as one of the reasons behind DEF as they provide voids that act as free space for the accumulation of DEF.

- Late Sulfate Release: Sulfate, in its varying forms, is an essential component of Portland cement. Thus, the cause of DEF occurrence is not the presence of sulfate, but rather its solubility. For instance, sulfate gypsum, as a highly soluble substance, is unlikely to have a late sulfate release. On the other hand, other sulfates in Portland cement have the tendency to cause late sulfate releases. Due to their low solubility, sulfates may remain in the hardened cement, but hydrate later to form secondary ettringite.

- Exposure to Water: Exposing concrete to water can cause the movement of reactant ions (such as SO^{-2}_4 and Ca^{+2}) to the microcracks, which results in the growth of ettringite crystals and consequently expansion.

1.3 Research Approach

Previous research has been conducted at the University of Maryland to prove the presence of DEF and further understand the factors that enhance its occurrence. Tests have been conducted on concrete specimens with varying factors to observe how each factor played into the presence of DEF (Amde,2013). The varying factors include varying potassium contents, types of fine aggregates, exposure conditions, and curing methods. This research has used test data from different experiments done by different students.

This research has focused on further understanding the time dependence of concrete expansion when DEF is present. The nonlinear curve of expansion versus time was fit into a nonlinear kinetics model developed by Feuze et al. (2019), shown below:

$$\varepsilon(t) - \varepsilon_o = A\left(1 - e^{-[K(t-t_o)]^n}\right)$$

Where:

A = Asymptotic expansion

k = Growth rate constant

n = Dimensionality

t_0 = Initial time lag

ε_0 = Expansion at t_0

The model describes the transformation kinetics of one phase to another as a function of time. In this context, it is used to describe how DEF influences the expansion of concrete due to DEF nucleation and growth.

Thus, the 4 parameters of the model provide a framework for comparing results of the various UMD DEF experiments.

Chapter 2: Literature Review

The natural mineral, ettringite, was first found in 1847 in limestone minerals in lava at Ettringen and Mayen in the Rhineland (Dana, 1932). It was first observed as a colorless mineral consisting of hexagonal crystals. In 1890, Candlot published a formula for the compound: $C_3A.3CaSO_4.32H_2O$.

Delayed ettringite formation was first recognized in the early 1980s when a new distress mechanism began causing cracking in railway ties in Europe. The same mechanism was also believed to be the cause of destructive cracking in other precast concrete products (Hime, 1996). The term “delayed ettringite formation” was first used by Heinz and Ludwig (1987) to refer to the ettringite that did not form in the early hydration of cement but later. Heinz and Ludwig conducted their research based on reports from both Germany and the US assigning DEF as a major cause of deleterious expansions in concrete structures. However, Day (1992) suggests that “secondary ettringite formation” is a more accurate term, since DEF “implies that conditions within the microstructure might be stable for the formation of ettringite but that ettringite does not form”, which is inaccurate. The issue of high-temperature curing, however, has remained a source of debate for many researchers. Day suggests that at high temperatures, ettringite may dissolve in the pore liquid of concrete. On the other hand, Heinz and Ludwig have proposed that primary ettringite is broken down to monosulfate at high temperatures. Monosulfate is then reconverted to ettringite when the concrete is exposed to moisture and normal temperatures.

In 1989, the Duggan test was proposed by Duggan and Scott to test the potential presence of ASR in concrete. Their paper concludes that a specimen subjected to the Duggan test experiences expansion that is a function of the percentage and form of sulfate in cement rather than alkali-aggregate reaction (AAR).

DEF has been found in many precast concrete structures, due to the practice of curing concrete at high temperatures (above 70℃) to accelerate construction and achieve strength at early stages. However, Rome and Sellevold (1994) have proposed that concrete cured at high temperatures shows lower strength than concrete cured at normal temperatures. They also conclude that, although Portland cement-based materials that are exposed to high temperatures (above 70°C) will stop forming ettringite, the ettringite that has been formed at an early stage will decompose to hydrated calcium monosulphoaluminate, moving sulfates to pores in the process (Rome and Sellevold, 1994). With the advancement of research, many studies have agreed that the moist conditions caused by curing concrete at high temperatures may result in the development of DEF. Heinz, Ludwig, and Rudinger (1989) conclude that steam curing at high temperatures causes the development of monosulphate, which converts to ettringite at later stages. However, some studies have drawn controversial conclusions. Stadelman's research concludes that ettringite decreases at temperatures above 60°C. Similarly, using energy-dispersive analysis X-ray (EDAX), Ronne and Hammer (1999) conclude that ettringite decreases as temperature increases from 20°C to 85°C. Because of these controversies, many worldwide standards and guidelines have been implemented. In Norway, for example, the standard stipulates that the heat of hydration remains below 65°C. Similarly, Germany specifies a heat of hydration at a

maximum of 60°C for exposed concrete structures (Scrivener, Damidot, and Famy,1999).

In 1987, Heinz and Ludwig conducted experiments to observe the presence of ettringite in heat-cured concrete using C3A at 12% by weight and SO3 at 3.8% by weight. Concrete was heat-treated at temperatures ranging from 20°C to 100°C. After curing, specimens were exposed to water at 20°C. Measurements for length change, weight change, and resonance frequency were taken periodically. Heinz and Ludwig (1987) report cracks forming from the edges due to the loss of bonds between cement paste and coarse aggregate. Finally, they conclude that heat-curing at temperatures equal to or above 70°C is linked with expansion, a decrease in strength, and an overly proportional increase in weight. They suggest that an increase in the temperature of the heat-curing leads to an increase in the factors that damage precast units.

Shayan (1996) concludes that in his research, DEF was developed under heat-curing temperatures of 75°C only if reactive aggregates were used.

Despite this substantial body of prior research, various uncertainties remain regarding the relationship between heat-curing at elevated temperatures and the occurrence of DEF. Many countries worldwide continue to impose standards and guidelines on heat-curing temperatures as reports of its relationship with deleterious expansion continue to increase.

Chapter 3: Test Procedures and Methodology

This research has utilized the data from research previously conducted at the University of Maryland, College Park, to test the applicability of the nonlinear kinetics model that shows the time dependence of the expansion of concrete due to DEF. The test methods were conducted on concrete specimens with varying cement chemistry, curing methods, and exposure conditions (Amde, 2013). Specimens were then subjected to heat cycles which are proven methods to initiate microcracks and DEF. Length and weight measurements were taken periodically. Laser Shearography, a nondestructive technique, was employed to trace cracking caused by DEF. Additionally, a scanning electron microscope (SEM) that utilizes energy dispersive analysis X-ray (EDAX) was used to monitor mineral deposits in cavities, transition zones, and microcracks.

The first task of this research consisted of compiling the datasets from these previous studies. The total number of projects carried in this program is about 12. However, it was not possible to obtain data from those theses and dissertations that exist only in hard copy because of the closure of the UMD libraries due to the Covid-19 epidemic. Ultimately, seven projects with usable data were found. Most of these contained multiple data sets. These are listed in **Tables 3.1 & 3.2**. It should be noted that the data in one study, Lijeron (2008) is reproduced in McMorris (2009), so there are actually only six independent data sets.

Table 3.1: Test Data Used in Research, Part I

Student	Degree	Date	Title
Amal Azzam	PhD	2002	Delayed Ettringite Formation in Steam-Cured Concrete, The Effect of Increasing Alkali Level and Exposure Conditions
Ken Williams	MS	2003	Influence of Fine Aggregate Lithology on Delayed Ettringite Formation in High Early Strength Concrete
Cintia Lijeron	MS	2008	Correlating Q-factor Measurements to Other Parameters in Deteriorated Concrete
Nicolas McMorris	PhD	2009	Linear and Non-linear Frequency Domain Techniques for Processing Impact Echo Signals to Evaluate Distributed Damage in Concrete

Table 3.2: Test Data Used in Research, Part II

Student	Degree	Date	Title
Jorgomai Ceesay	PhD	2007	Characterization of Damage in Mortar and Concrete Specimens Due to Delayed Ettringite Formation
Newman & Amde (SBIR Report)	n/a	2011	Development of Prototype Compact Shearography System, Analysis Method and Software for Micro-Crack Detection
Serge Feuze	PhD	2019	The Influence of Thermal Cycles and Potassium on the Damage Mechanics of Delayed Ettringite Formation

These projects can be classified into two categories based on their objectives. The first category, which consists three studies, Azzam (2002), Williams (2003) and Ceesay (2007), investigated the effect of various factors on the DEF damage mechanics itself. The other category concerned the evaluation of nondestructive test methods for DEF including ultrasonics (McMorris, 2009), laser shearography (Newman, 2011) and neutron tomography (Feuze, 2019). In these cases, test specimens with representative amounts of DEF damage were prepared.

The available data sets came in three different forms. In some cases, they consisted of the original data spreadsheets. In others, they were presented as tables in documents.

These all contained the mean values of the expansion data for the replicate prisms, but the associated standard deviations were not always included. Finally, some cases existed only in the form of graphs. The data were extracted from these graphs using digitization software.

A detailed description of each of the datasets, including the experiments and tests conducted; specimens' chemistry; specimens' exposure conditions; and curing methods, is provided in the sections below.

3.1 Jorgomai Ceesay's Data

Ceesay's research was conducted in 2004 to characterize the damage that occurs in concrete specimens due to DEF. Ceesay prepared concrete prisms measuring 3" x 3" x 11.25" in accordance with ASTM C109-99 and C305-99.

The end of each prism was equipped with two steel gauge studs used to monitor length change. The specimens were divided into two batches: the first was considered a control specimen with no varying parameters, while the second contained an additional potassium carbonate (K_2CO_3) content added to water to facilitate expansion (Ceesay, 2007). The total potassium content in the mix was 1.5%. Both batches were steam-cured. Different specimens were then exposed to different exposure conditions. The concrete prisms' chemistry included the following:

3.1.1 Portland Cement Type III

Portland cement Type III is characterized by a relatively high sulfate content and a higher heat hydration, both of which are proven factors in inducing the formation of

ettringite. A chemical analysis of cement which was measured by an X-ray fluorescence spectrometry is shown in **Table 3.3**.

Table 3.3: Chemical Analysis of Type III Portland Cement

Chemical Analysis of Cement	
Analyze	Weight %
SiO_2	19.88
Al_2O_3	5.03
Fe_2O_3	2.79
CaO	61.79
MgO	2.51
SO_3	3.89
Na_2O	0.31
K_2O	0.82
TiO_2	0.21
P_2O_5	0.17
Mn_2O_3	0.07
SrO	0.20
Cr_2O_3	< .01
ZnO	0.02
L.I.O (950°C)	2.01
Total	99.67
Alkalis as Na_2O	0.85
Calculated Compounds per ASTM C150-02	
C_3S	51
C_2S	18
C_3A	9
C_4AF	8
ss($C_4AF + C_2F$)	--

3.1.2 Sand

Ceesay's specimens have also consisted of manufactured Fredrick Stone Sand in accordance with ASTM C33-99a. Frederick Stone Sand has a moisture absorption rate of 1.0% and a specific gravity of 2.69.

3.1.3 Coarse Aggregate

Limestone aggregate was used with a specific gravity of 2.72, a dry rodded weight of 102.3 lb/ft^3, and a moisture absorption rate of 3%.

3.1.4 Potassium Carbonate (K_2CO_3)

To increase the potassium content of the second batch, anhydrous granular grade potassium carbonate was used.

The mixing proportion of each batch is shown in **Table 3.4**.

Table 3.4: Mixing Proportions of Two Concrete Batches (referred to in Ceesay's research as Phases 3 and 4)

	PHASE 3						PHASE 4					
Mix	I	II	III	IV	V	VI	I	II	III	IV	V	VI
Water (lb)	30.0	30.0	30.0	33.8	33.8	48.8	30.0	30.0	30.0	33.8	33.8	48.8
Cement (lb)	60.0	60.0	60.0	67.5	67.5	97.6	60.0	60.0	60.0	67.5	67.5	97.6
C. Aggregate (lb)	129.2	129.2	129.2	145.4	145.4	210.0	129.2	129.2	129.2	145.4	145.4	210.0
F. Aggregate (lb)	59.3	59.3	59.3	88.9	88.9	128.4	59.3	59.3	59.3	88.9	88.9	128.4
Added P. Carbonate by wt. of cement (lb)	-	-	-	-	-	-	0.52	0.52	0.52	0.58	0.58	1.14

3.1.5 Treatment Conditions

All specimens were steam-cured. While in steel molds, specimens were placed in a water bath in an oven at a temperature of 85°C for two (2) hours and then at a temperature of 85°C for four (4) hours. They were then left to cool overnight before being stored underwater at room temperature for six (6) days. Specimens were then subjected to heat cycles which are proven ways to initiate microcracks (Ceesay, 2007).

3.1.5.1 Heat Cycles

The heat cycle consists of three sub-cycles. In the first two cycles, specimens are placed in a dry oven at a temperature of 82°C for one (1) day; the specimens are then left to cool for 1.5 hours before being placed in water at room temperature for one (1) day. The third cycle consists of the specimens being placed in a dry oven at a temperature of 82°C for three (3) days, after which they are left to cool at room temperature for two (2) days. Specimen expansion is then monitored and recorded for up to 100 days. The heat cycle is shown in **Figure 3.1**

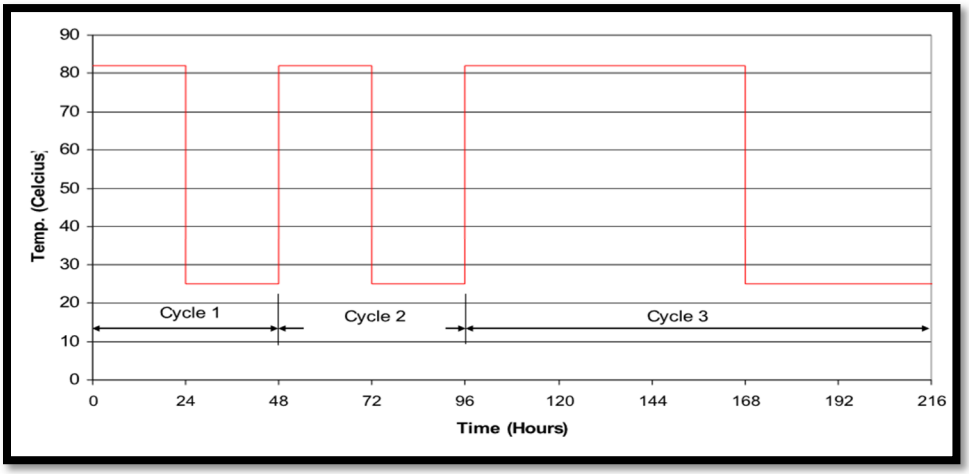

Figure 3.1: Heat Cycle for Concrete Specimens

3.1.6 Storage Conditions

Concrete prisms were stored in different storage containers, each with different storage conditions:

3.1.6.1 Exposure Condition 1: Isothermal Water Bath, pH of 12.5

This storage condition consisted of a saturated solution of calcium hydroxide and water at room temperature with a pH maintained at 12.5. Concrete specimens were completely immersed in the solution.

3.1.6.2 Exposure Condition 2: Plain Water at Room Temperature

This storage condition consisted of regular tap water at room temperature. Specimens were also completely immersed.

3.2 Nicolas McMorris' Data

Nicolas McMorris (2009) performed similar experiments to Jorgamai Ceesay but with different varying conditions. Two batches of 3" x 3" x 11.25" prisms were prepared; Batch 1 was considered the control batch (no additional potassium carbonate content), while Batch 2 contained a total of 2.06% potassium carbonate per weight of cement. Both batches were subjected to heat cycles. Mixing proportions of Nicolas McMorris' specimens are shown in **Table 3.5**. Note that this table excludes additional potassium carbonate added.

Table 3.5: Nicolas McMorris' Mixing Proportions for Specimens

Constituent	Weight
Water	*24.89 lb*
Cement	*49.74 lb*
Coarse Aggregate	*111.6 lb*
Fine Aggregate	*81.62 lb*

Similarly to Ceesay's materials, the cement used was Portland cement Type III, while the coarse aggregate was limestone aggregate with a 1" maximum diameter. Fine aggregates were the Frederick stone sand, while the potassium used was anhydrous granular reagent-grade potassium carbonate.

All specimens were steam-cured in a conventional oven at a temperature of 85℃ for four hours. After curing, all specimens were submerged in storage containers containing lime water for eighteen (18) days. Specimens were then subjected to either the heat cycles or freeze-thaw cycles before being returned to storage containers containing limewater.

3.3 Kenneth Williams' Data

Kenneth Williams' research was published in 2003 at the University of Maryland, College Park. While previous research by Ceesay and McMorris focused on varying the potassium content in concrete specimens, the scope of Williams' research focused on varying fine aggregates based on their ASR ratings. Williams used the same type of

cement used in previous experiments, namely Portland cement Type III; the coarse aggregate used was the dolomitic limestone. Additionally, the potassium carbonate used as an admixture was the anhydrous granular reagent-grade potassium carbonate.

3.3.1 Silver Hill Fine Aggregate

Silver Hill is considered a highly expansive type of fine aggregate, with a higher ASR rating than the two other types of fine aggregates used in Williams' experiments. The physical characterization of the fine aggregates used is shown in **Table 3.6**.

3.3.2 Millville Fine Aggregate

Selected for the control specimen, the Millville fine aggregates have a relatively small ASR rating of (0.028%). This type of sand is milled from quarried limestone gravel (Williams, 2003).

5.1.3 Brandywine Fine Aggregate

Brandywine fine aggregates have a mild ASR rating of 0.14%. The sand is a product of sedimentary rock collected from water streams and is considered coarse compared to other types of sands.

Table 3.6: Physical Characterizations of Fine Aggregates used in Williams' Tests

NAME	MILLVILLE	BRANDYWINE	SILVER HILL
ORIGIN	MILLVILLE QUARRY, INC.	E.L. GARDENER, INC.	SILVER HILL MATERIALS
CERTIFICATION DATE	25-Apr-02	20-Feb-02	31-May-02
METHOD OF PRODUCTION	MANU. SAND FROM MANU. GRAVEL	MANU. SAND FROM NATURAL GRAVEL	NATURAL SAND
SIEVE ANALYSIS			
3/8"	100%	97%	100%
#4	97%	6%	97%
#8	94%	2%	83%
#30	55%	0.90%	47%
#50	23%	0.75%	22%
#200	1.50%	0.30%	1.20%
PHYSICAL PROPERTIES			
ABSORPTION (ASTM C-128)	0.66%	1.20%	0.90%
BULK SP GRAVITY (ASTM C-128)	2.826	2.59	2.61
SOUNDNESS (ASTM C-88) MAGNESIUM SULFATE	4.259% LOSS	2.73% LOSS	1.3% LOSS
ASR	0.028%	0.14%	0.28%
PETROGRAPHIC EXAMINATION			
	87.1% DOLOMITIC LIMESTONE 7.3% LIMESTONE	UNKNOWN VARIES	85.3% QUARTZ 8.9% QUARTZOSE SANDSTONE 1.5%CHALCEDONIC CHERT

3.3.4 Sample Preparation

Three different batches were prepared, each with a different type of fine aggregate. **Table 3.7** provides a brief description of each batch. All samples consisted of a potassium content of 1.50% by weight of cement and a water-to-cement ratio of 0.50. Additionally, all specimens were steam-cured after casting. Steam-curing involved placing the specimens in an oven at a temperature of 85℃ for four (4) hours. Specimens were then submerged in lime water at room temperature and left for seven (7) days to continue curing. Finally, samples were exposed to heat cyclse, after which they were placed in long-term storage.

Table 3.7: Batch Details Used by Williams

	BATCH #1	BATCH #2	BATCH #3
Fine Aggregate	Silver Hill	Millville	Brandywine
Date Cast	8/15/2002	8/22/2002	8/28 - 8/29/2002
Exposure Conditions	WET/SAT.	WET/SAT./SUB.	WET/SAT.
Total Cylinders	22*	32*	20
Total Prisms	27*	30	20

3.4 Amal Azzam's Data

Similarly to Ceesay and McMorris, Azzam studied the effect of increasing potassium content on concrete expansion in the absence of ASR. Similarly, Portland cement Type III, limestone coarse aggregate, and anhydrous granular reagent potassium carbonate were used. Fine aggregates conforming to ASTM C33 were also used.

3.4.1 Specimen Preparation

Three concrete batches were prepared. The first batch was considered the control batch with no additional potassium content added, relying only on the potassium from cement which comprises approximately 0.72% of its weight. 1% and 2% of potassium carbonate were added to the second and third batches, respectively, thereby increasing the potassium content to 1.4% and 2.1%, respectively. All specimens were steam-cured after 2 hours. Steam-curing consisted of heating for four (4) hours at a temperature of 85℃. Specimens were then left to cool down overnight before being stored under water

at room temperature. A week later, specimens were subjected to heat cycles, after which, they were stored either under water or left in the air.

3.5 Newman & Amde (SBIR Report) Data

For the Phase II SBIR, two batches of concrete specimens were created. Batch 1 (TX1) was considered the control specimen and had no additional potassium content added. In Batch 2 (TX2), an additional potassium content was added for a total potassium content of 1.2% per weight of cement. **Table 3.8** shows the materials used to cast the specimens.

All specimens were steam-cured, as shown in **Figure 3.2**. After curing, specimens were subjected to heat cycles.

Table 3.8: SBIR Report Specimen Materials

Mix	Batch 1 (TX1)	Batch 2 (TX2)
Water		
Cement	Type III	Type III
Coarse Aggregate	Limestone #57	Limestone #57
Fine Aggregate	Texas Sand - Alkali Reactivity 0.05	Texas Sand - Alkali Reactivity 0.05
K_2CO_3	-	Total 1.2%
No. of Prisms	9	9
No. of Cylinders	12	12

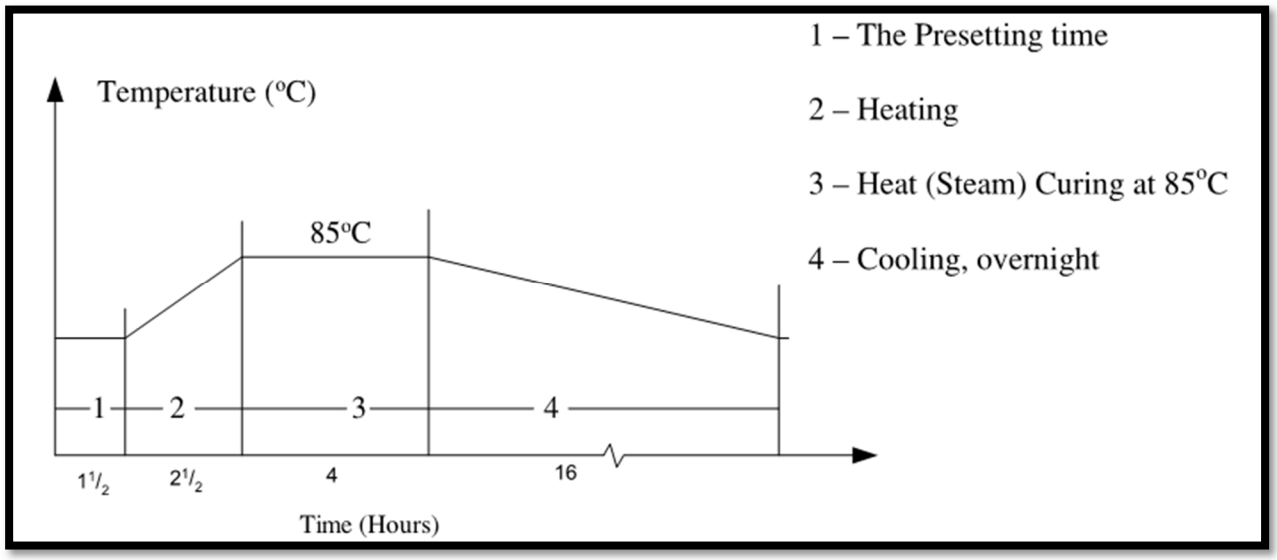

Figure 3.2: Steam-Curing Treatment for Concrete Specimens

Chapter 4: Nonlinear Kinetics Model Tools

All of the datasets discussed in the previous chapter were fit into a nonlinear model to test the applicability of the model developed by Serge et al. (2019) on a certain set of factors. A description of the model, along with the tools used, is shown below.

4.1 DEF Expansion Model Stages

According to Serge et al. (2019), the weakening of specimens exposed to heat occurs in three different stages when plotting expansion versus time, as shown in **Figure 4.1**.

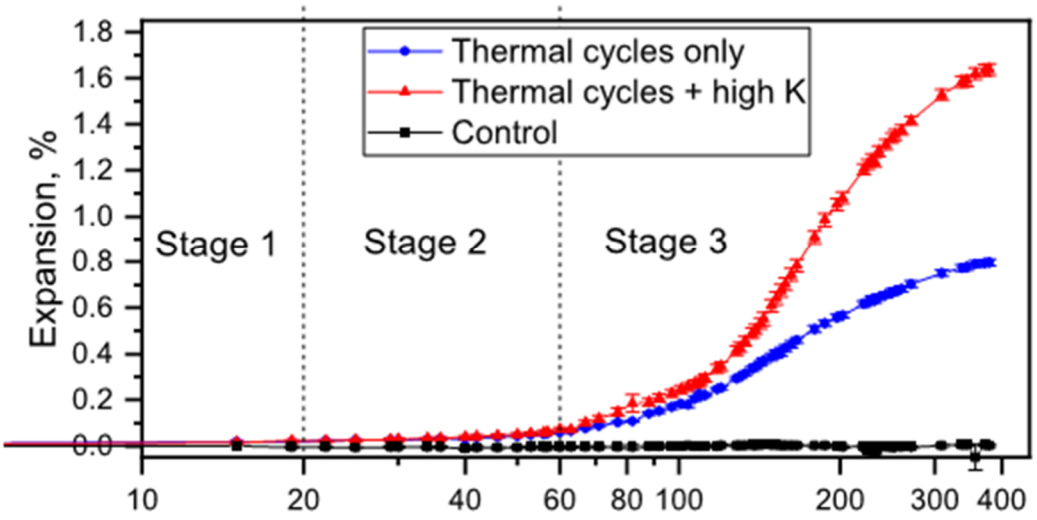

Figure 4.1: Three Stages of DEF Damage Progression

4.1.1 Stage 1

Stage 1 is often referred to as the pore filling stage. From day 0 to day 20, ettringite is forming but does not result in specimen expansion, as it is merely filling the available pore space. The specimen experiences an increase in weight only.

4.1.2 Stage 2

This stage is known as the creep stage, during which a correlation between the increase in weight and expansion can be observed. Most of the pores have become filled with ettringite and start to swell, creating creep stress. However, as the concrete's resistance to creep stresses is still low at this stage, it is able to accommodate these stresses.

4.1.3 Stage 3

Stage 3 begins after 60 days and is known as the crack propagation stage. At this point, concrete resistance to creep stresses advances, and significant expansion is witnessed as weight increases. Additionally, ettringite continues to settle in what have now developed to be wide cracks. As the cracks widen, the available moisture facilitates the growth of ettringite crystals, which in turn leads to more cracking. Consequently, a decrease in the specimen's compressive strength is also witnessed as microcracks and voids become interconnected.

4.2 Nonlinear Kinetics Model

The data of the third stage of the expansion model was fit to the nonlinear kinetics model. The model describes the kinetics of phase transformation through a plot of the change in volume versus the time of phase growth. It describes the transformation of a solid specimen from one stage to another and provides a clear description of the kinetics of crystallization. Transformations are often observed as S-shaped curves with

a low rate of transformation in the beginning and the end and a higher rate in the middle.

This model has been developed to describe the formation of DEF in concrete specimens. It also identifies different expansion mechanisms occurring at different time intervals. The model parameters are shown below:

$$\varepsilon(t) - \varepsilon_o = A\left(1 - e^{-[K(t-t_o)]^n}\right)$$

Where:

ε(t) = Expansion at time t

ε_0 = Expansion at t_0

A = Asymptotic expansion coefficient

K = Rate constant

t = Time

n = Dimensionality

4.2.1 Rate Constant *K*

The rate constant *K* refers to the growth rate of ettringite in the concrete specimen, thus describing the rate at which reactions are occurring. According to Feuze et al. (2019), the rate constant K does not depend on the number of initial cracks nor the amount of water pouring into these microcracks.

4.2.2 Asymptotic Expansion Coefficient *A*

In this model, the parameter *A* was introduced as the asymptotic expansion coefficient to scale the data. It is a characteristic of the number of cracks that were initiated in the specimen as part of the pre-heat treatment; “It is the limiting value for ε(t) when *t* goes to infinity” (Feuze et al., 2019).

4.2.3 Dimensionality *n*

The dimensionality parameter *n* describes the transformation that occurs in a concrete specimen during expansion. According to Feuze et al. (2019), an *n* value of 1 indicates that the transformation happens along a line, *n* = 2 indicates that change is occurring through a surface, and *n* = 3 indicates that transformation occurs through a volume. The larger the value of *n*, the greater the density of the microcracks caused by the pre-heat treatments.

4.3 OriginPro 2020b

Results from previous tests were fit to the nonlinear kinetics model using the software OriginPro 2020b. The fitting function builder shown in **Figure 4.2** was used to enter the model equation along with the parameters. “y_0” represents expansion at “t_0”. Parameters *A* and *K* were pre-set at 0.8 and 0.0075, respectively, but these were not set as fixed variables. Parameter *n* was determined through a trial-and-error method, where n was changed based on the best fit. The fit was then performed using OriginPro’s nonlinear curve fit tool, shown in **Figure 4.3**. Several fitting iterations were then performed until the optimal fit was achieved.

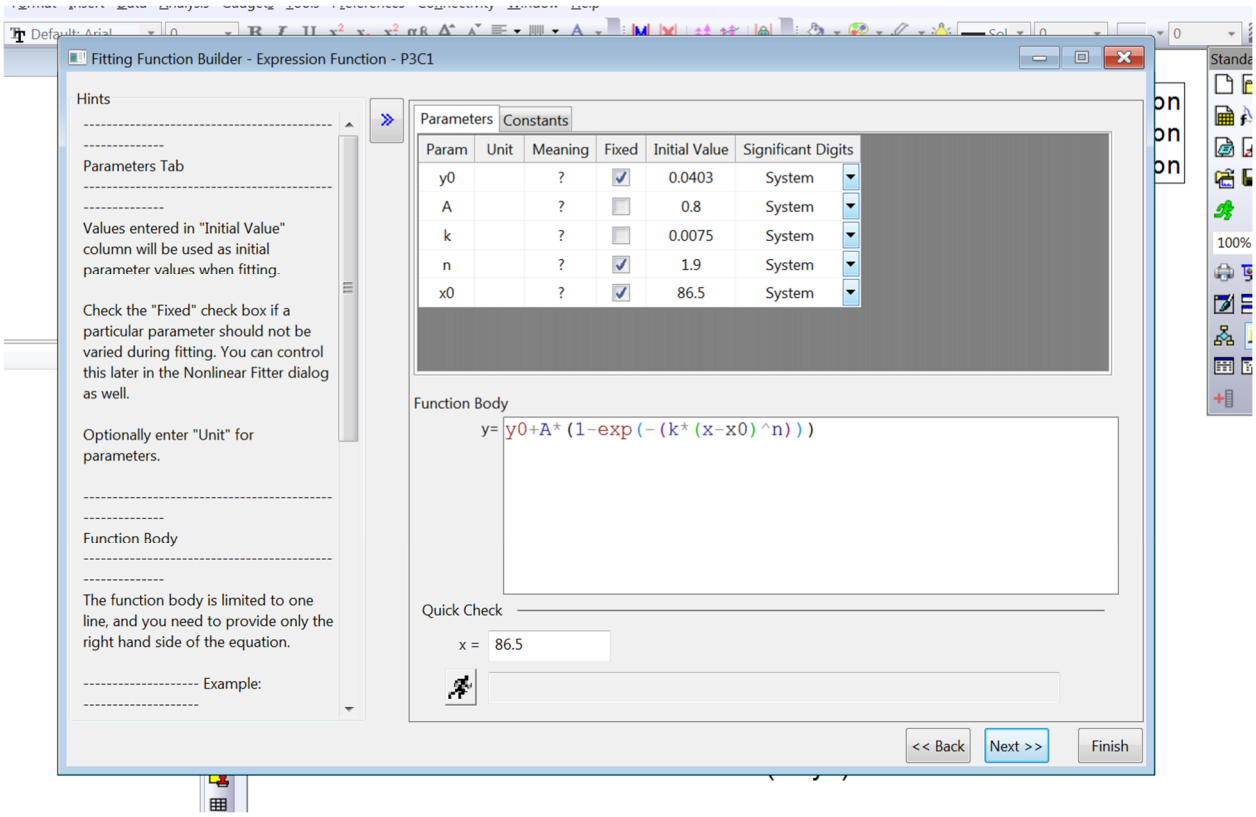

Figure 4.2: OriginPro Function Builder Window

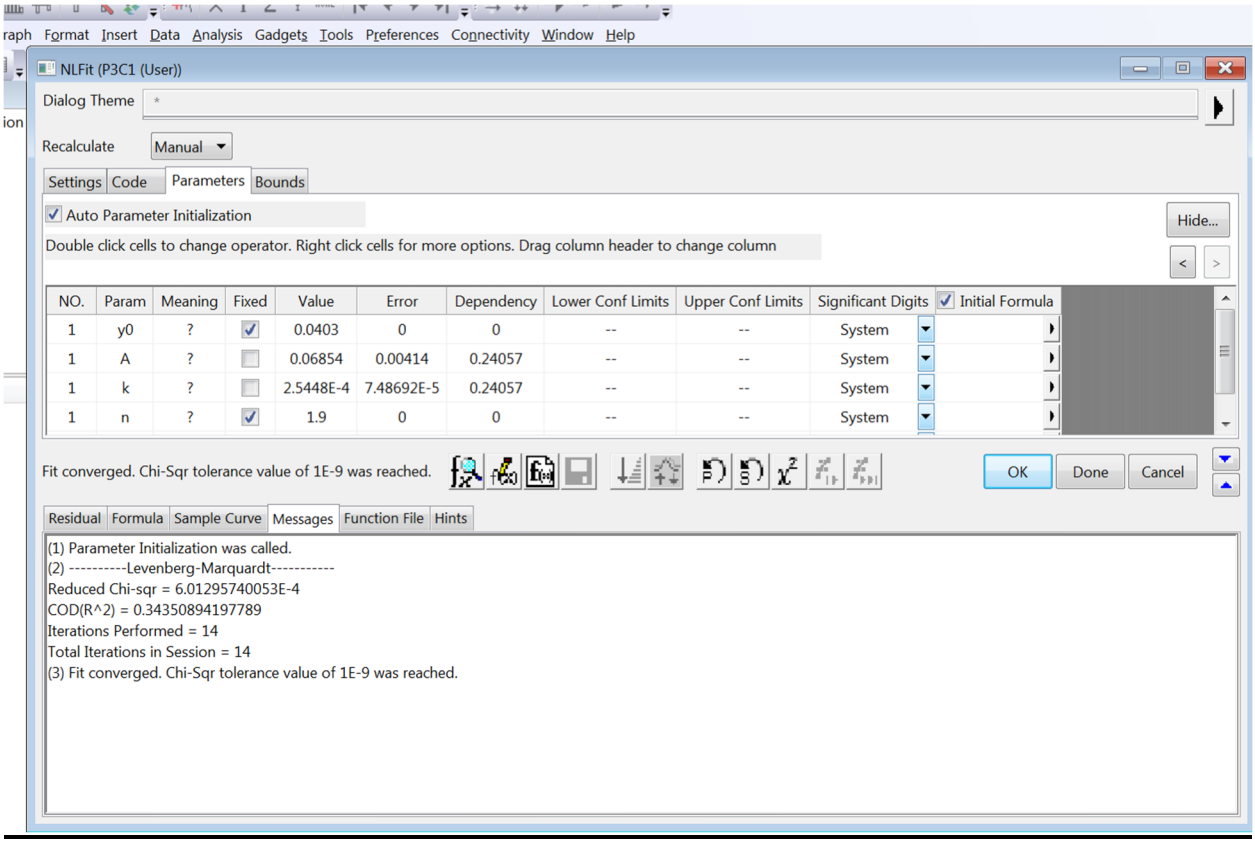

Figure 4.3: OriginPro Nonlinear Curve Fit Window

Chapter 5: Results

5.1 Jorgomai Ceesay

5.1.1 Batch 1:

Table 5.1: Batch 1 Specimen and Nonlinear Fit Details

Batch 1 Details	
Chemistry	No Added Potassium
Curing	Steam-Curing
Treatment	Heat Cycle
Exposure Condition	Isothermal Water Bath pH at 12.5
A	1.06
K	1.91E-05
n	1.9

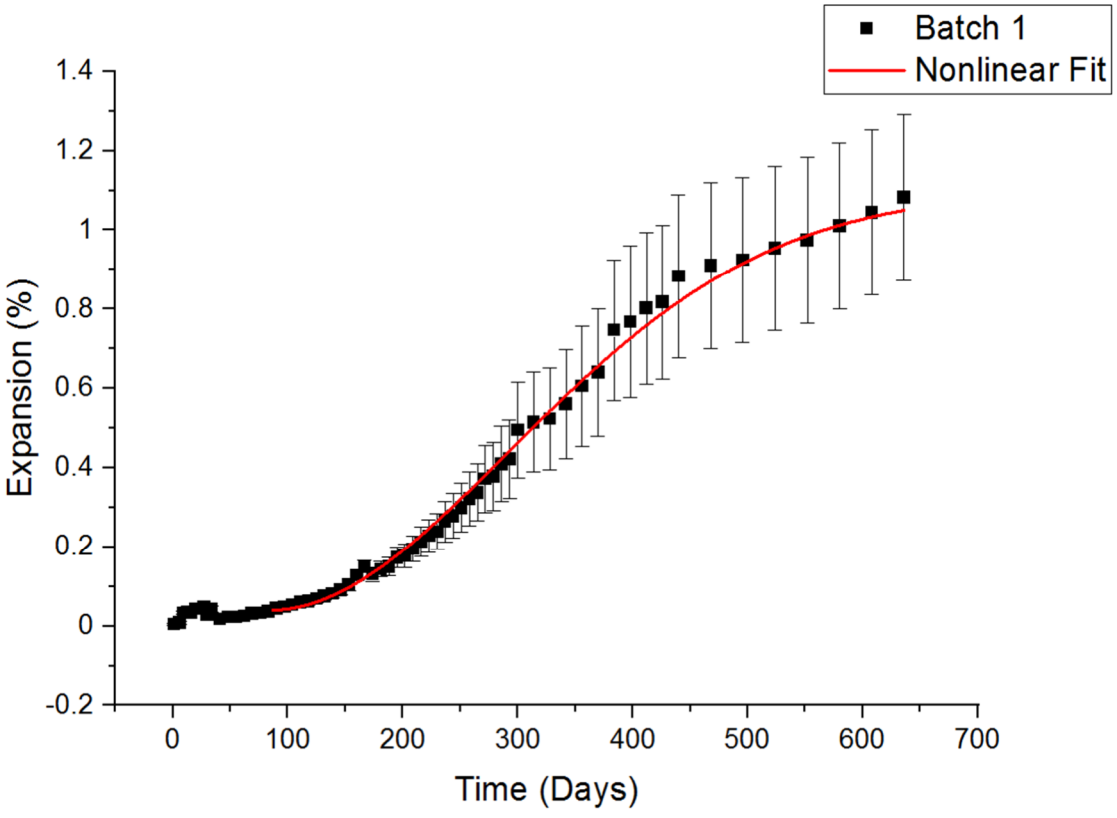

Figure 5.1: Batch 1 Expansion Vs. Time Graph

5.1.2 Batch 2:

Table 5.2: Batch 2 Specimen and Nonlinear Fit Details

Batch 2 Details	
Chemistry	No Added Potassium
Curing	Steam-Curing
Treatment	Heat Cycle
Exposure Condition	Plain Water at room temperature
A	0.71
K	2.20E-03
n	1.2

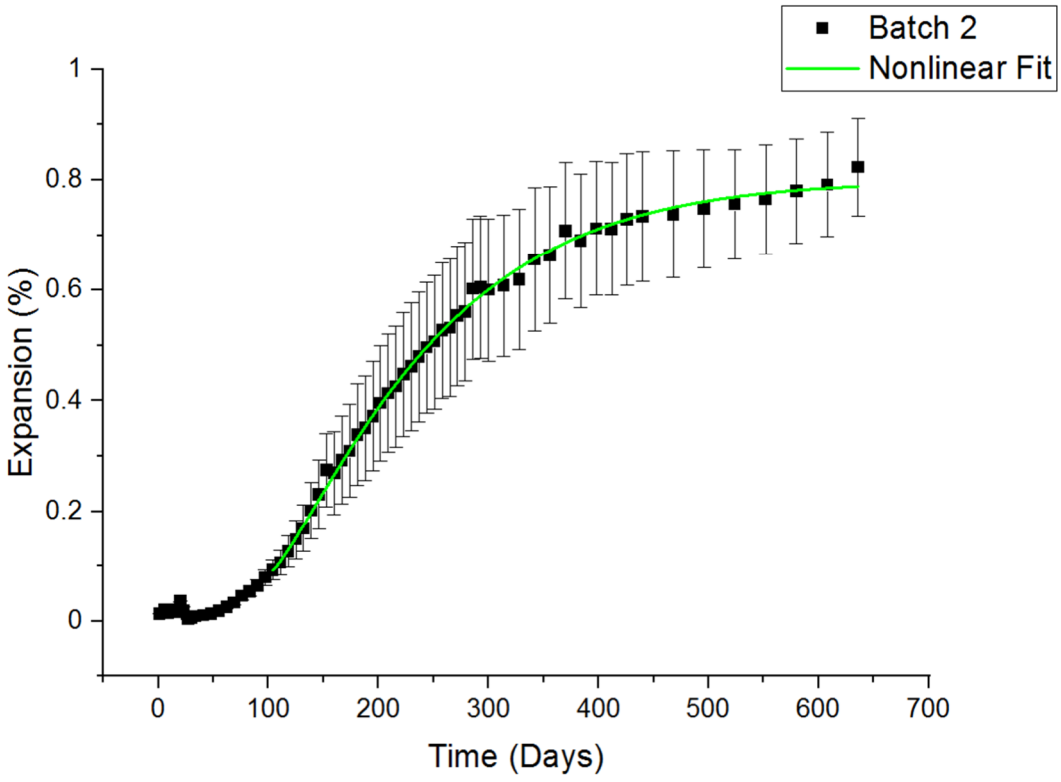

Figure 5.2: Batch 2 Expansion Vs. Time Graph

5.1.3 Batch 3:

Table 5.3: Batch 3 Specimen and Nonlinear Fit Details

Batch 3 Details	
Chemistry	1.5% Total Potassium Content
Curing	Steam-Curing
Treatment	Heat Cycle
Exposure Condition	Isothermal Water Bath pH at 12.5
A	1.25
K	3.62E-05
n	1.9

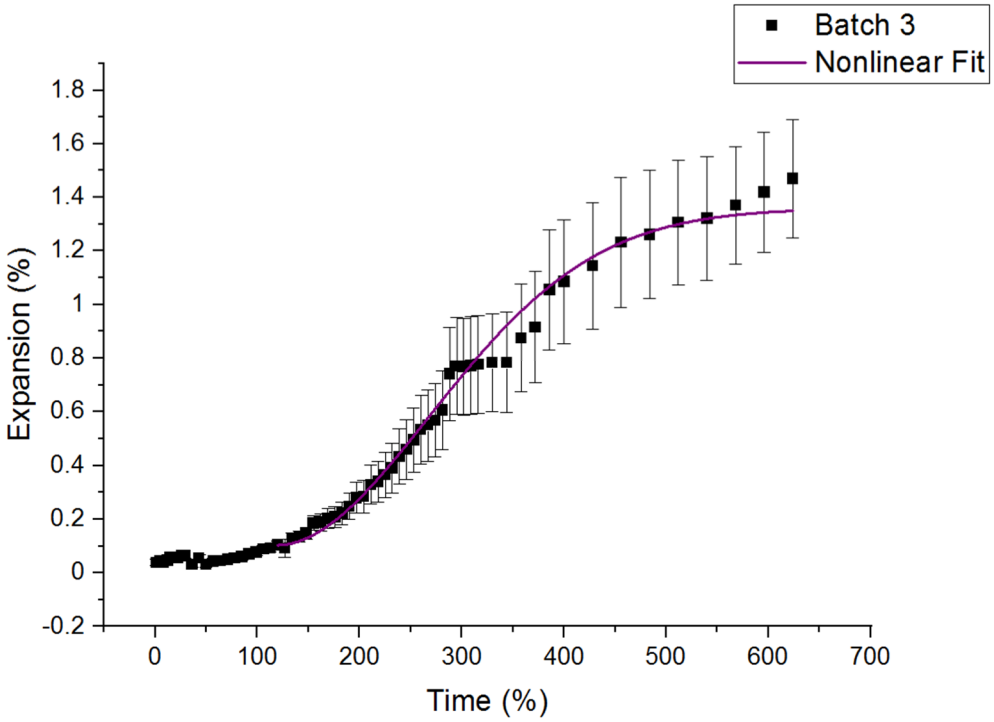

Figure 5.3: Batch 3 Expansion Vs. Time Graph

5.1.4 Batch 4:

Table 5.4: Batch 4 Specimen and Nonlinear Fit Details

Batch 4 Details	
Chemistry	1.5% Total Potassium Content
Curing	Steam-Curing
Treatment	Heat Cycle
Exposure Condition	Plain Water at room temperature
A	1.37
K	7.63E-05
n	1.8

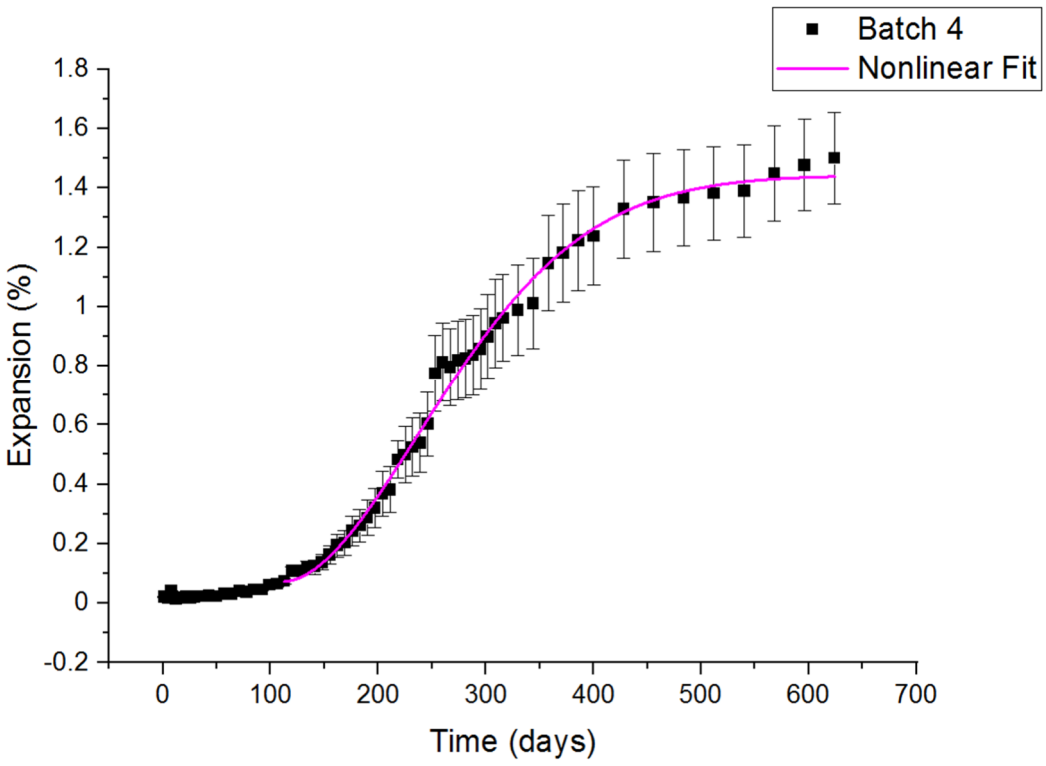

Figure 5.4: Batch 4 Expansion Vs. Time Graph

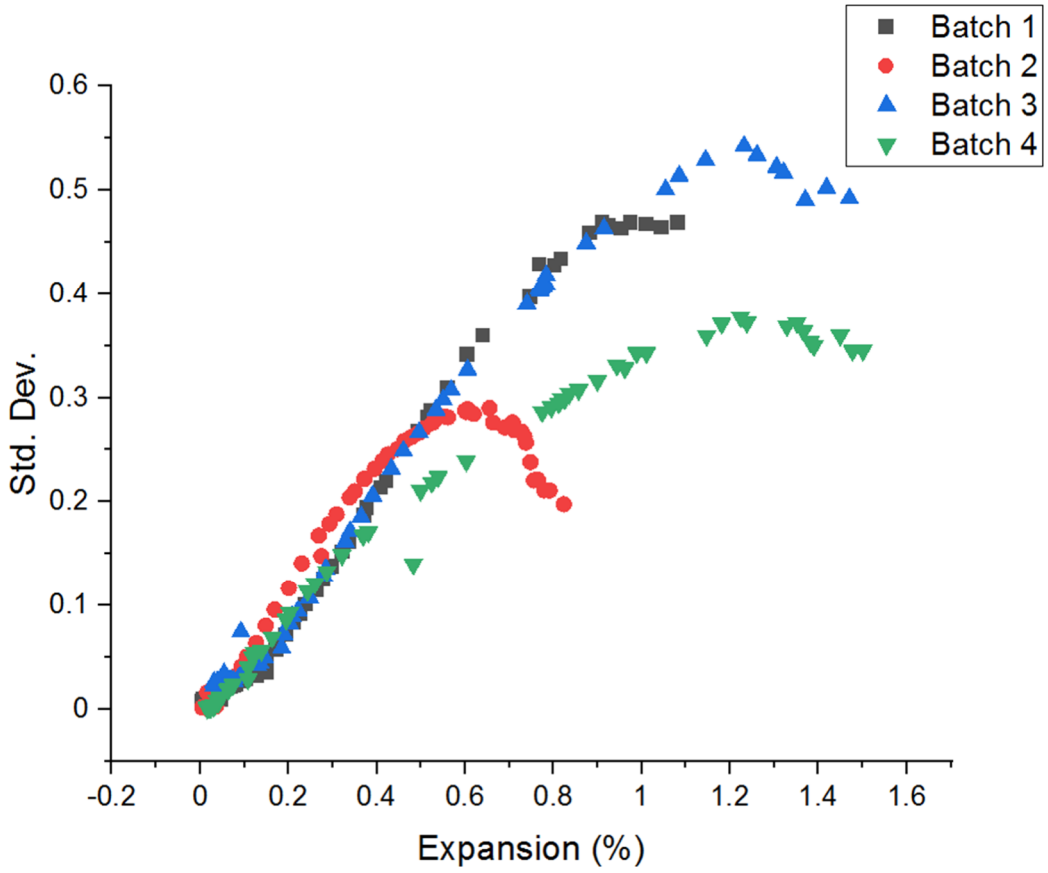

Figure 5.5: Standard Deviation Vs. Expansion of All Batches

5.2 Nicolas McMorris:

Table 5.5: Batches 1 and 2 Specimens and Nonlinear Fit Details

Batch 1 Details	
Chemistry	Control (No Potassium Added)
Curing	Steam-Curing
Treatment	Heat Cycle
Exposure Condition	Limewater
A	0.1
K	1.12E-01
n	-0.001
Batch 2 Details	
Chemistry	2.1% Total Potassium Content
Curing	Steam-Curing
Treatment	Heat Cycle
Exposure Condition	Limewater
A	1
K	1.10E-03
n	0.85

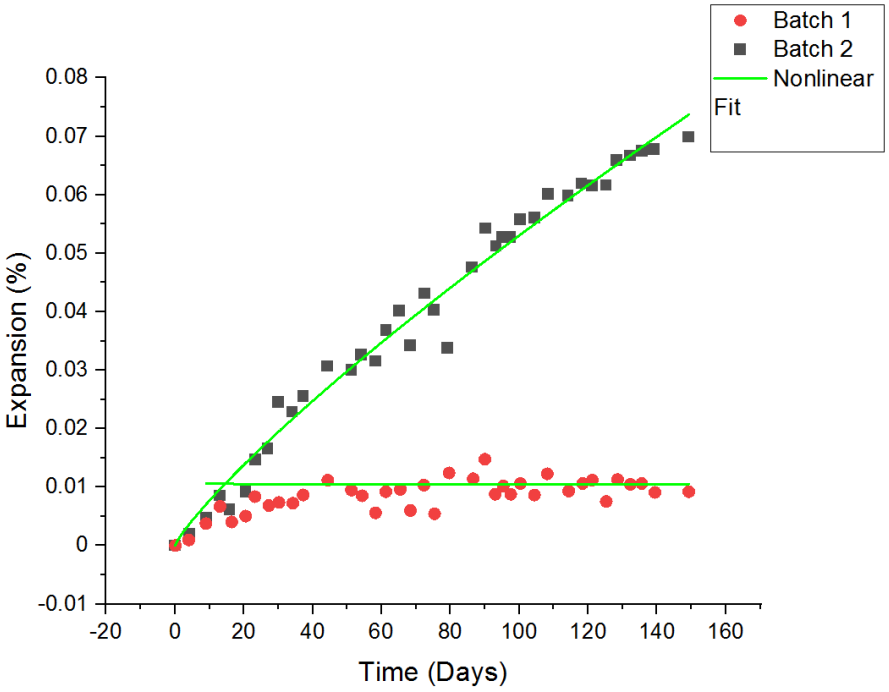

Figure 5.6: Batches 1 and 2 Expansion Vs. Time Graph

5.3 Kenneth Williams:

5.3.1 Batch 1:

Table 5.6: Batch 1 Specimens and Nonlinear Fit Details

Batch 1A Details	
Mix	High ASR Fine Aggregates
Curing	Steam-Curing
Treatment	Heat Cycle
Exposure Condition	Limewater
A	0.62
K	1.47E-05
n	2.5
Batch 1B Details	
Mix	High ASR Fine Aggregates
Curing	Steam-Curing
Treatment	Heat Cycle
Exposure Condition	100% Humidity
A	0.46
K	4.65E-08
n	3.7

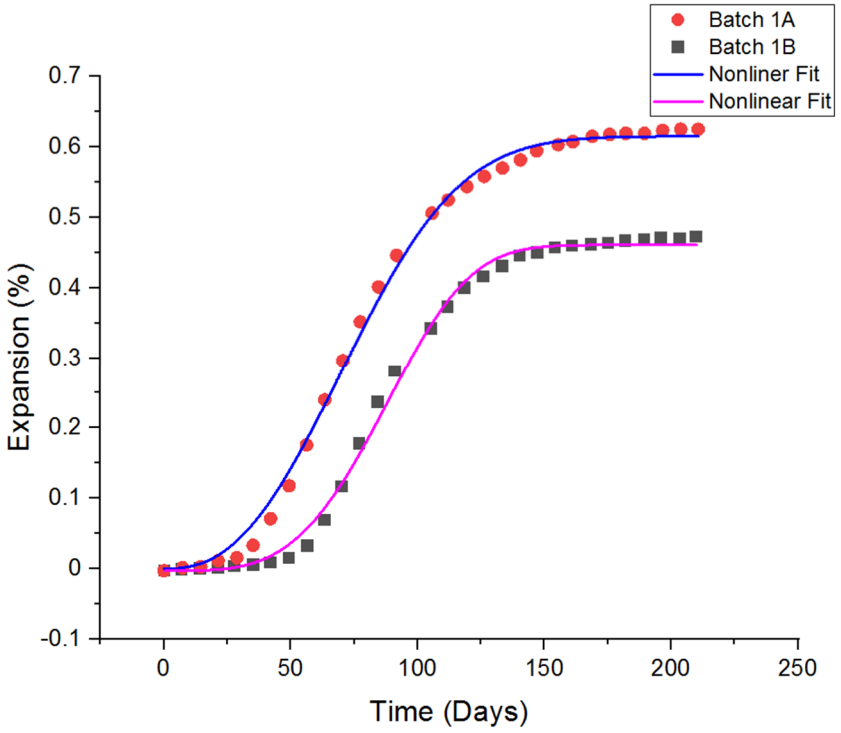

Figure 5.7: Batch 1 Expansion Vs. Time Graph

5.3.2 Batch 2:

Table 5.7: Batch 2 Specimens and Nonlinear Fit Details

Batch 2A Details	
Mix	Low ASR Fine Aggregates
Curing	Steam-Curing
Treatment	Heat Cycle
Exposure Condition	Limewater
A	0.12
K	1.32E-09
n	4.5
Batch 2B Details	
Mix	Low ASR Fine Aggregates
Curing	Steam-Curing
Treatment	Heat Cycle
Exposure Condition	100% Humidity
A	0.05
K	5.74E-09
n	4

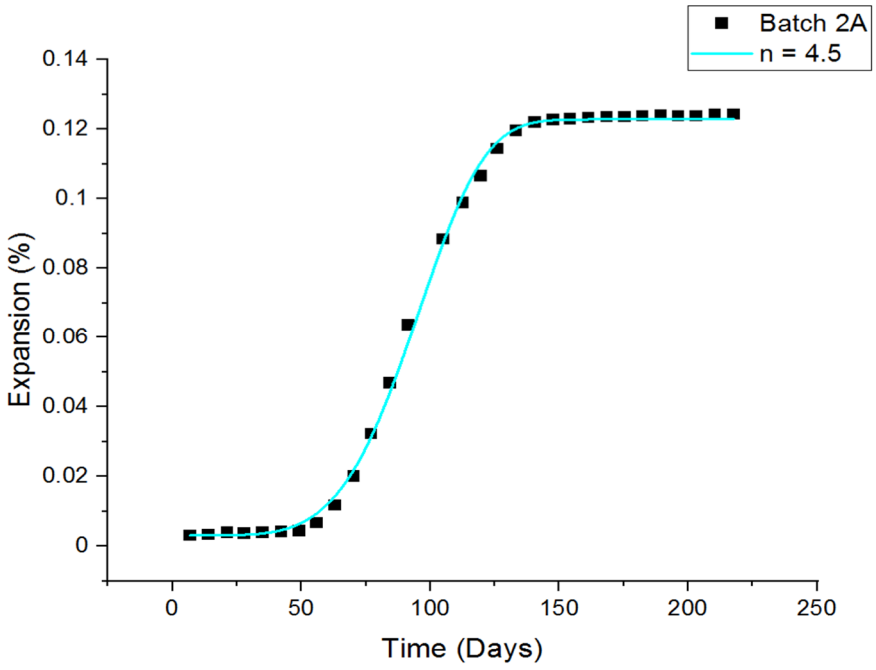

Figure 5.8: Batch 2A Expansion Vs. Time Graph

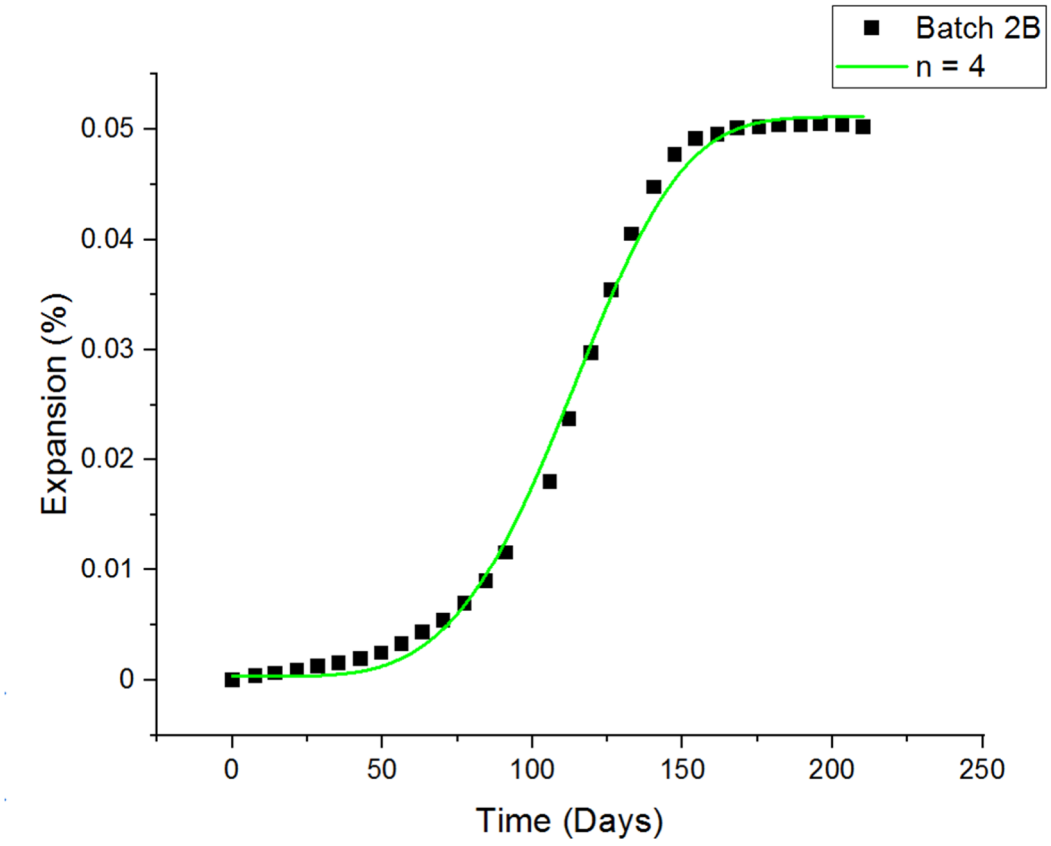

Figure 5.9: Batch 2B Expansion Vs. Time Graph

5.3.3 Batch 3:

Table 5.8: Batch 3 Specimens and Nonlinear Fit Details

Batch 3A Details	
Mix	Mild ASR Fine Aggregates
Curing	Steam-Curing
Treatment	Heat Cycle
Exposure Condition	Limewater
A	0.49
K	1.22E-07
n	3.5
Batch 3B Details	
Mix	Mild ASR Fine Aggregates
Curing	Steam-Curing
Treatment	Heat Cycle
Exposure Condition	100% Humidity
A	0.25
K	6.14E-07
n	3.2

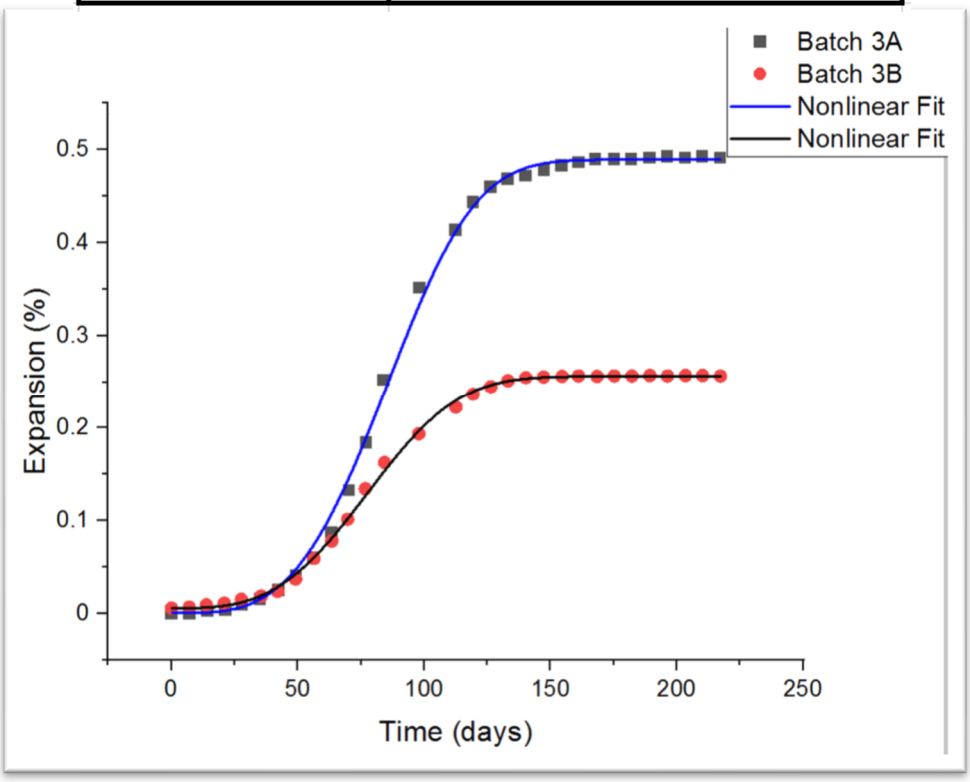

Figure 5.10: Batch 3 Expansion Vs. Time Graph

5.4 Azzam and Newman & Amde (SBIR):

Table 5.9: Specimens and Nonlinear Fit Details

SBIR (TX1) Details	
Chemistry	0.57% Total Potassium Content
Curing	Steam-Curing
Treatment	Heat Cycle
Exposure Condition	Water
A	0.1
K	2.54E-03
n	1.2
SBIR (TX2) Details	
Chemistry	1.2% Total Potassium Content
Curing	Steam-Curing
Treatment	Heat Cycle
Exposure Condition	Water
A	2.9
K	6.02E-04
n	0.8
Azzam (Batch1) Details	
Chemistry	1.4% Total Potassium Content
Curing	Steam-Curing
Treatment	Heat Cycle
Exposure Condition	Water
A	0.49
K	3.18E-05
n	1.8
Azzam (Batch2) Details	
Chemistry	2.1% Total Potassium Content
Curing	Steam-Curing
Treatment	Heat Cycle
Exposure Condition	Water
A	0.86
K	1.29E-04
n	1.8

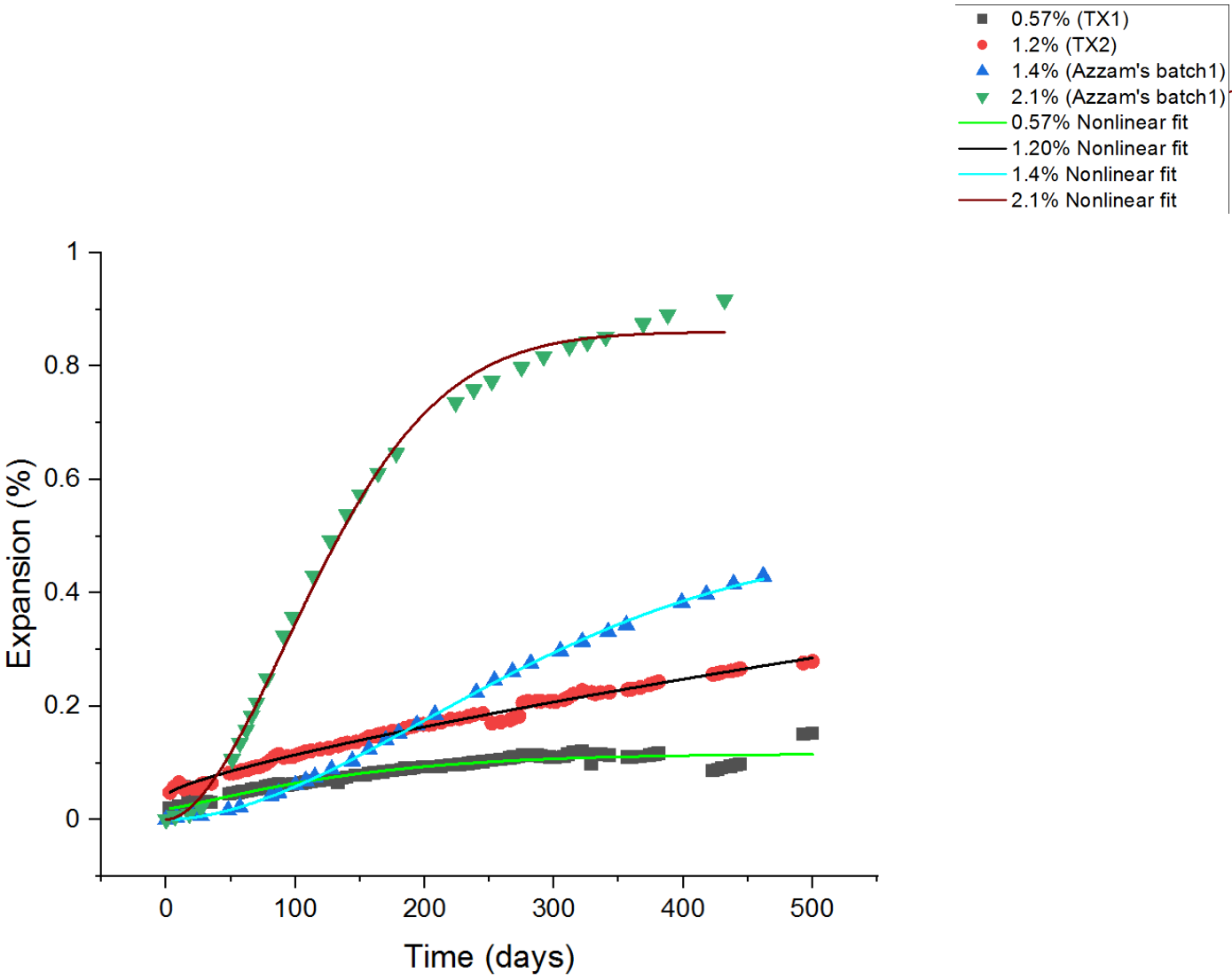

Figure 5.11: Expansion Vs. Time Graph

Chapter 6: Discussion of Results

As mentioned previously, each of the nonlinear kinetics model parameters refer to certain expansion characteristics that indicate the behavior of each specimen given the varying factors. This section will discuss the results observed in Chapter 5 in the order that they were presented. The next chapter will draw overall conclusions on the relationships observed.

6.1 Jorgamai Ceesay Discussion of Results

Table 6.1, shown below, provides a visual comparison of the values obtained from the previous chapter.

As mentioned in previous sections, parameter *k* refers to the rate at which growth and expansion occurs in the specimen. The smallest *k* value was observed in specimens of Batch 1, which is the control specimen with no additional potassium content. This indicates a slower rate of growth and nucleation. However, the rate of growth increases when specimens are stored in plain water, as in Batch 2.

This observation is also consistent when examining the *k* values of Batches 3 and 4. The rate of growth has nearly doubled in specimens of Batch 4 in comparison to those of Batch 3.

However, the nonlinear fit for Batch 2 showed a higher *k* value than all other batches. Batch 2 was also considered a control specimen; however, it was stored in plain water at room temperature after the heat cycle, whereas Batch 1 was placed in an isothermal

water bath. This indicates that specimens' exposure to plain water at room temperature can induce nucleation and growth.

"The coefficient *A* is the limiting value for $\mathcal{E}(t)$ when *t* goes to infinity" (Serge et al. 2019). Thus, parameter *A* should reflect the amount of microcracks that were generated by increasing the potassium content or exposing the specimens to the heat cycle. As shown in **Table 6.1**, Batches 3 and 4 have higher *A* values than Batches 1 and 2. Although all batches were exposed to heat cycles, Batches 3 and 4 contain a higher potassium content, which explains their higher *A* value.

When studying the effect of exposure conditions, however, no relation can be found between storage conditions and parameter *A*. When specimens were exposed to plain water in Batch 2, a lower *A* value was observed than in specimens in Batch 1. Conversely, exposure to plain water led to an increase in *A* in Batch 4.

Parameter *n* refers to the dimensionality of the specimen's transformation. Like parameter *A*, *n* is also a factor of the amount of microcracks initiated. It is necessary to note that all specimens were exposed to heat cycles, thus making potassium content and exposure conditions the only varying factors. By examining **Table 6.1**, it is evident that no relation is found between these varying factors and the value of *n*. Batches 1, 3, and 4 have similar n values of 1.9 and 1.8, indicating that the transformation occurs through the surface, whereas the value of *n* in Batch 2 indicates that transformation occurs through a line.

Table 6.1: Ceesay's Parameter Value Comparisons

Ceesay's Parameter Value Comparisons	
Batch 1	
A	1.06
K	1.91E-05
n	1.9
Batch 2	
A	0.71
K	2.20E-03
n	1.2
Batch 3	
A	1.25
K	3.62E-05
n	1.9
Batch 4	
A	1.37
K	7.63E-05
n	1.8

6.2 Nicolas McMorris

Table 6.2: McMorris' Parameter Value Comparison

Mcmorris's Parameter Value Comparisons	
Batch 1	
A	0.1
K	1.12E-01
n	-0.001
Batch 2	
A	1
K	1.10E-03
n	0.85

The initial nonlinear fit results for McMorris' data yielded significantly low values of *A* which is not physically possible. This might be due to the fact that the nonlinear fitting routine can yield physically implausible values when the initial values of the parameters are far off from the true values. For this reason, parameter *A* was set at a certain value for this fitting activity, while *k* and *n* varied, yielding the results shown in **Table 6.2**. Parameter *A* in Batch 2 was higher than Batch 1, which indicates that additional microcracks formed in specimens with higher potassium content.

However, a higher *k* value is observed for specimens with low potassium contents (i.e. Batch 1), which is an unlikely result. Furthermore, the dimensionality parameter, *n*, shows a negative value in Batch 1.

It is important to note that McMorris' experiment was conducted over a shorter period of time (about 160 days) in comparison with the rest of the experiments presented in this research. Although the data were fit using the nonlinear fit model, the Expansin vs time plot does not exhibit a completely nonlinear behavior since the nonlinear behavior often occurs later in the process.

6.3 Kenneth Williams

A comparison of the model parameters is shown in **Table 6.3.**

Table 6.3: Williams' Parameter Value Comparisons

Williams's Parameter Value Comparisons	
Batch 1A	
A	0.62
K	1.47E-05
n	2.5
Batch 1B	
A	0.46
K	4.65E-08
n	3.7
Batch 2A	
A	0.12
K	1.32E-09
n	4.5
Batch 2B	
A	0.05
K	5.74E-09
n	4
Batch 3A	
A	0.49
K	1.22E-07
n	3.5
Batch 3B	
A	0.25
K	6.14E-07
n	3.2

Specimens of the same batch that had different exposure conditions had significantly varying parameters. The highest *k* value was observed in specimens of Batch 1A, which had the highest ASR rating. Specimens in Batch 2A, which contained the lowest ASR

rating in the experiment, showed the lowest *k* values in comparison with the other batches. This is because the fine aggregates used in Batches 2A and 2B were the least expansive aggregates in the experiment, thus resulting in a small growth rate. Consequently, specimens in Batches 3A and 3B showed *k* values that are in the middle since the fine aggregates used for Batch 3 have mild ASR ratings. It is also important to note that the specimens that were stored in 100% humidity had higher rates of growth (i.e., higher *k* values) than those stored in limewater. This demonstrates that storing specimens in 100% humidity after exposing them to the heat cycles induces a faster growth rate.

The lowest *A* values were observed in Batches 2A and 2B. As mentioned in earlier sections, parameter *A* is a factor of the number of microcracks initiated in the experiment through varying factors. In this particular experiment, all specimens were subjected to the heat cycle; however, the type of fine aggregates and exposure conditions were different. Thus, the lowest *A* value was observed in the specimens with the lowest ASR fine aggregate. Consequently, specimens with high ASR fine aggregates, namely Batches 1A and 1B, had the highest *A* values, while the values of Batches 3A and 3B were between the two extremes. This indicates that a higher ASR value of fine aggregates would result in the initiation of a higher number of microcracks, which is consistent with the conclusions drawn in Kenneth Williams' paper (2003). Furthermore, specimens exposed to lime water after the heat cycle had higher *A* values than the specimens exposed to 100% humidity, which indicates that limewater enhanced the initiation of microcracks.

The highest *n* values are observable in Batches 2A and 2B, as shown in **Table 6.3**. This suggests that microcracks are denser in specimens with low ASR aggregates.

While all specimens had dimensionality values that indicated that transformation occurred throughout a volume, a higher *n* value indicates denser microcracks, which was observed with specimens with low ASR aggregates.

However, it is important to consider that there was no relation found between storage conditions and the value of *n*. When specimens were stored in limewater in Batches 2A and 3A, the nonlinear fit showed higher *n* values than when specimens were stored in 100% humidity. On the other hand, when specimens were stored in limewater in Batch 1A, the nonlinear fit showed lower *n* values.

6.4 Azzam and Newman & Amde (SBIR)

Table 6.4: Azzam and SBIR Parameter Value Comparisons

SBIR & Azzam's Parameter Value Comparisons	
SBIR (TX1)	
A	0.1
K	2.54E-03
n	1.2
SBIR (TX2)	
A	2.9
K	6.02E-04
n	0.8
Azzam's Batch 1	
A	0.49
K	3.18E-05
n	1.8
Azzam's Batch 2	
A	0.86
K	1.29E-04
n	1.8

When comparing Azzam's Batch 1 and Batch 2 parameters, a relationship can be identified between the varying factors and the parameters. Azzam's Batch 1 consists of 1.4% total potassium content, while Batch 2 consists of 2.1% total content. A higher *k* value is observed in Batch 2, indicating a higher rate of growth than specimens in Batch 1. This is consistent with earlier findings that a higher potassium content results in a higher rate of ettringite growth.

Furthermore, the nonlinear fit showed a higher *A* value in Batch 2, indicating that a higher number of microcracks was generated when potassium content increased. Since both batches have the same *n* value, it can be concluded that varying potassium content does not influence the dimensionality of the specimens' transformation.

The nonlinear fits of TX1 and TX2 in the SBIR report, however, showed varying results in comparison to Azzam's, although the only varying factor was the potassium content (0.57% total potassium content in TX1 and 1.2% in TX2). The nonlinear fit of TX2 was expected to show lower *A* and *K* values since specimens have lower potassium contents. Yet, higher values were observed. This is potentially attributable to the fact that the material suppliers were different since both were completely independent experiments. It is also important to note that Azzam's experiment was conducted approximately a decade before the SBIR report.

Chapter 7: Conclusions

7.1: Research Conclusions

It can be concluded from the results presented in this research that the nonlinear kinetics model previously developed by Feuze et al. (2019) on a certain set of factors can be applied to other DEF experiments with a range of varying factors. Thus, the model provides a framework for comparing the effects of various factors on the presence of DEF.

This research has used the Levenberg-Marquardt method which provides an efficient way to fit multiple variables of a nonlinear curve concurrently. The method works through a nonlinear curve fit by the line of steepest descent. However, there are certain situations where the resulting parameter values are not physically possible.

In experiments where standard deviation and mean expansion data were available, the coefficient of variation plot was obtained, as shown in **Figure 5.5** in **Chapter 5**. The graph showed a linear dependence of the standard deviation on the mean expansion which is a common characteristic of overall volumetric expansion of prims. Eventually, however, this relation is interrupted as the standard deviation becomes independent of the mean expansion or homoscedastic, suggesting a transition to different forms of damage mechanics.

Table 7.1: Summary Table

Data	Batch #	Total K_2O%	A Strain, %	K $1000^{-1}Days^{-1}$	n	t_o Days
Ceesay	1	0.82%	1.06	0.02	1.9	86.5
	2	0.82%	0.71	2.20	1.2	104
	3	1.50%	1.25	0.04	1.9	120
	4	1.50%	1.37	0.08	1.8	113
Mcmorris	1	0.56%	0.1	112.00	-0.001	0.123
	2	2.06%	1	1.10	0.9	0
Azzam	1	1.40%	0.49	0.03	1.8	0
	2	2.10%	0.86	0.13	1.8	0
SBIR	TX1	0.57%	0.1	2.54	1.2	3
	TX2	1.20%	2.9	0.60	0.8	3
Williams	1A	1.50%	0.62	0.01	2.5	0.292
	1B	1.50%	0.46	0.00	3.7	0.171
	2A	150%	0.12	0.00	4.5	6.89
	2B	1.50%	0.05	0.00	4	7.69
	3A	1.50%	0.49	0.00	3.5	0.119
	3B	1.50%	0.25	0.00	3.2	0.0595
Feuze	1	0.79%	0.86	7.00	1.2	N/A
	2	1.50%	1.69	7.50	1.6	N/A

Notes:

1. All specimens were steam-cured except Feuze's specimens which were cured in a moist room.
2. All specimens were exposed to heat cycles.
3. Batches 1A&1B in Williams' data consist of high ASR fine aggregates.
4. Batches 2A&2B in Williams' data consist of low ASR fine aggregates.
5. Batches 3A&3B in Williams' data consist of mild ASR fine aggregates.

Table 7.1 shows a summary of results presented in the previous section. While some results varied from one experiment to another, certain conclusions can be drawn from the nonlinear fit parameter values.

It can be deduced from the values of parameter *A* shown in **Table 7.1** that *A* is sensitive to both potassium contents and temperature during early age concrete. It tends to increase when a specimen's potassium content is increased. Additionally, both steam-curing and the heat cycles enhance the initiation of microcracks and increase their volume, providing more space for ettringite to grow.

Furthermore, *A* tends to increase when highly expansive fine aggregates are used in a specimen, as seen in Williams' experiments.

Regarding the impact of exposure conditions on the amount of microcracks initiated, conclusions drawn can vary significantly. In some experiments such as Ceesay's, storing specimens in limewater helped to initiate microcracks when no additional potassium content was added; similarly, less microcracks were initiated when specimens had additional potassium. On the other hand, specimens stored in limewater showed higher *A* values than those stored in 100% humidity, as seen in Williams' experiments. **Figure 7.1** shows the plot of *A* vs K_2O. Although specimens differ in exposure conditions, a relationship can be seen between the potassium content and the value of *A*.

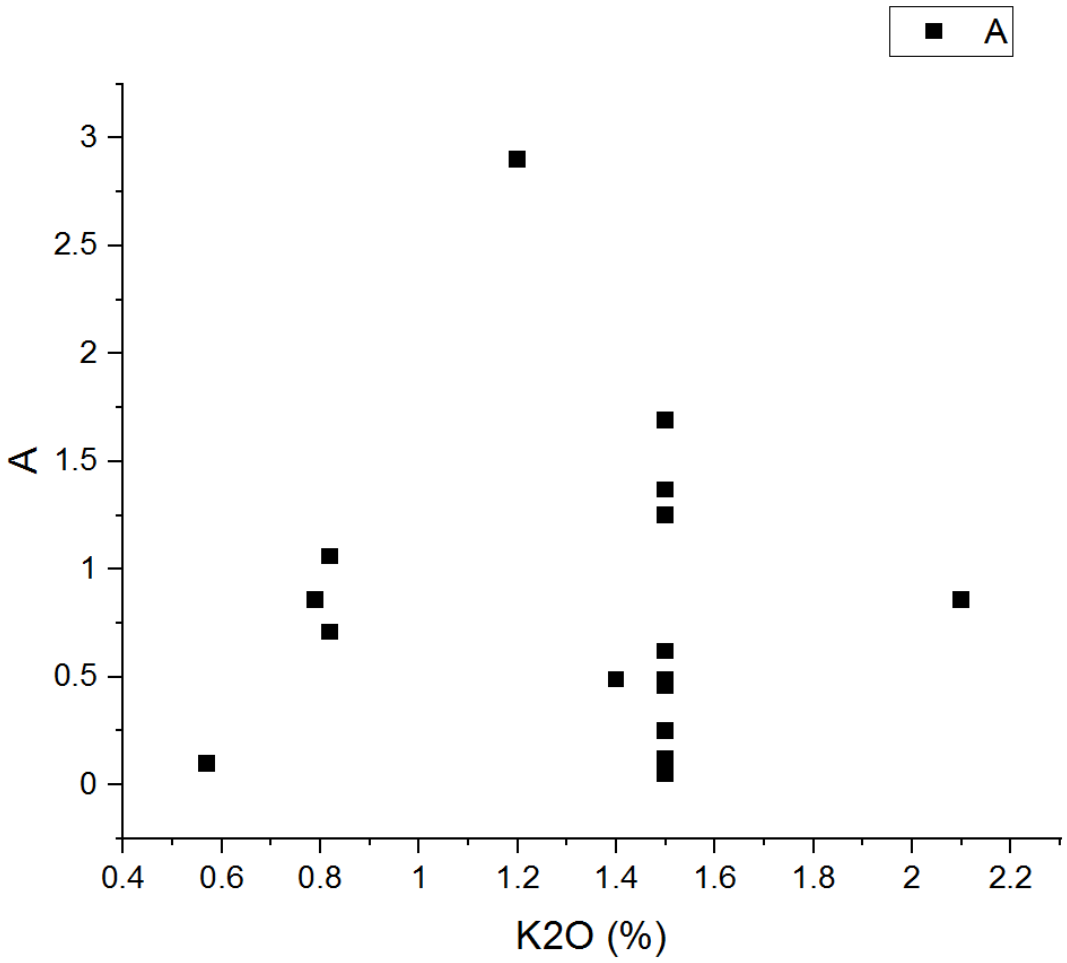

Figure 7.1: *A* Vs. K_2O

The rate of growth and nucleation values (i.e., parameter *k*) also varied significantly from one experiment to another. While it was expected that the rate of growth would increase in correlation with the specimen's potassium content, this was not always the case. Its variation may be related to variations in the cement chemical composition. **Figure 7.2** shows the plot of k vs K_2O.

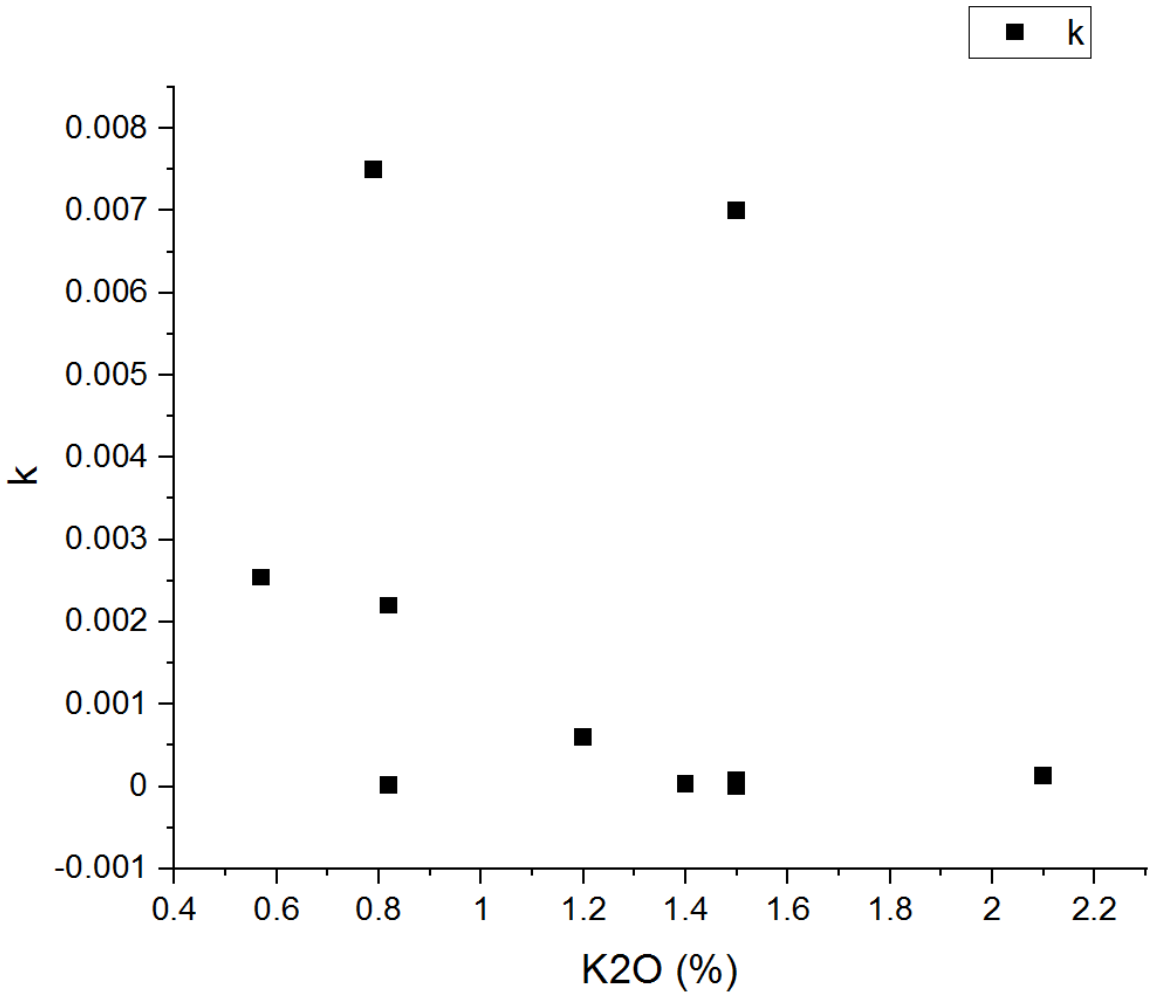

Figure 7.2: *k* Vs. K_2O

No relationship was found between the dimensionality of the transformation of one crystal to another, i.e., parameter *n*, and varying factors. As seen in McMorris' experiments among many others, specimens with different potassium contents had highly similar *n* values. It has been observed, however, that for most steam-cured specimens that have been exposed to the heat cycle, change occurs through the surface. Instead, when fine aggregates with varying ASR ratings were used, transformation occurred throughout a volume.

Additionally, no relationship was found between the dimensionality of change and the different storage conditions, as indicated in **Table 7.1**

7.2: Future Research

This research has primarily focused on testing the applicability of the nonlinear kinetics model on DEF experiments previously done by the University of Maryland. The varying factors of these experiments were primarily varying potassium contents and different types of fine aggregates. Further research should be conducted on a nonlinear kinetics model of a wider range of factors that influence DEF. Furthermore, a focus on the variation of cement chemical composition is necessary to further understand the rate of ettringite growth.

References

1. Feuze, S., Livingston, R. A., & Amde, A. M. (2019). The Influence of Thermal Cycles and Potassium on The Damage Mechanics of Delayed Ettringite Formation. Retrieved from https://www.researchgate.net/publication/333888615_The_Influence_of_Thermal_Cycles_and_Potassium_on_the_Damage_Mechanics_of_Delayed_Ettringite_Formation

2. Bollmann, K. & Stark, J. (1997). Untersuchungen zur späten Ettringitbildung im erhärteten Beton. Tagungsband vol. 13, pp. 1-0039 - 1-52.

3. Yan, P., Zheng, F., Peng, J. & Qin, X. (2004). Relationship between delayed ettringite formation and delayed expansion in massive shrinkage-compensating concrete, Cement and Concrete Composites, vol. 26, no. 6, pp. 687-93.

4. Williams, K. L. (2003). Influence of Fine Aggregate Lithology on Delayed Ettringite Formation in High Early Strength Concrete.

5. Hooton, R.D., Boyd, A.J. & Bhadkamkar, D. (2005). Effect of Cement Fineness and C3S Content on Properties of Concrete: A Literature Review, Portland Cement Association.

6. Collepardi, M. (1999). Damage by Delayed Ettringite Formation. Concrete International.

7. Dana, E. S. (1932). A Textbook of Mineralogy. Wiley and Sons.

8. Candlot, E. (1890). Properties des ciments et des liants hydrauliques, Bull. Soc. Encour. Ind. Natn., pp. 682-685

9. Hime, William G. (1996). Delayed Ettringite Formation - A Concern for Precast Concrete? PCI Journal.

10. Heinz, D., and Ludwig, U. (1987). Mechanisms of Secondary Ettringite Formation in Mortars and Concretes Subjected to a Heat Treatment. Bryant and Katherine Mather Symposium, American Concrete Institute SP-100, Scanlon, J., Editor, pp. 2059-2071.

11. Day, R. L. (1992). The Effects of Secondary Ettringite Formation on the Durability of Concrete. A literature Analysis of Portland Cement Association.

12. Duggan, R. and Scott F. (1989). New Test for Deleterious Expansion in Concrete. Alkali-Aggregate Reaction. 8th International Conference, Elsevier Applied Science. pp. 403-408.

13. Rome, M., and Sellevold, E. J. (1994). LIGTCON.DP2 Material Properties. Report 2.3 Effect of Hydration Generated Temperature-Literature Survey. SINTEF report STF70 A978424. Trondheim (in Norwegian).

14. Heinz, D., and Ludwig, U., and Rudinger, I. (1989). Delayed Ettringite Formation in Heat-Treated Mortar and Concretes. Concrete Precasting Plant and Technology, Vol. 11, pp. 56-61.

15. Ronne, M., and Hammer, T. A. (1999). Delayed Ettringite Formation (DEF) in Structural Lightweight Aggregate Concrete: Effect of Curing Temperature, Moisture, and Silica Fume Content. Cem. Concrete, and Aggregates, CCAGDP, Vol. 21, No. 2, pp. 202-211.

16. Scrivener, K. L., and Damidot, D., and Famy, C. (1999). Possible Mechanisms of Expansion of Concrete Exposed to Elevated Temperatures During Curing (Also Know as DEF) and Implications for Avoidance of Field Problems. Cement, Concrete, and Aggregates, CCAGDP, Vol. 21, No. 1, pp. 93-101.

17. Shayan, A. and Ivanusec, I. (1996). An Experimental Clarification of the Association of Delayed Ettringite Formation with Alkali Aggregate Reaction. Cem.Concr. Comp., Vol. 18, pp. 161-170.

18. Amde, A. M. and R. A. Livingston (2013). University of Maryland Studies on Delayed Ettringite Formation. International Conference on Advances in Cement and Concrete Technology in Africa. H. C. Uzoegbo. Johannesburg, South Africa, University of Witswatersrand**.**

19. Ceesay, J. (2007). Characterization of Damage in Mortar and Concrete Specimens Due to Delayed Ettringite Formation (DEF).

20. McMorris, N. (2009). Linear and Non-Linear Frequency Domain Techniques For Processing Impact Echo Signals To Evaluate Distributed Damage in Concrete.

21. Azzam, A., Amde, A. M., & Livingston, R. A. (2002). Delayed Ettringite Formation in Steam-Cured Concrete, The Effect of Increasing Alkali Level, and Exposure Conditions.

22. Newman, J. and Amde, A. M. (2011, March 24). Development of Prototype Compact Shearography System, Analysis Method and Software for Micro-Crack Detection. (Contract Number DTRT57-08-C-10001), SBIR Report, USDOT – FHWA, 104 pages.